

**VORTEX-INDUCED MOTIONS OF FLOATING OFFSHORE WIND TURBINES WITH FOUR CIRCULAR COLUMNS: A REDUCED ORDER MODEL ASSESSMENT OF SMALL-SCALE EXPERIMENTS IN A TOWING TANK**

**Éverton L. Oliveira<sup>1</sup>, Celso P. Pesce<sup>1a</sup>, Giovanni A. Amaral<sup>1,2</sup>,  
Hideyuki Suzuki<sup>3</sup> and Rodolfo T. Gonçalves<sup>3</sup>**

<sup>1</sup>Offshore Mechanics Laboratory, <sup>a</sup>Department of Naval Architecture and Ocean Engineering, Escola Politécnica, University of São Paulo, Av. Prof. Lúcio Martins Rodrigues, Butantã, São Paulo, 05508-020, Brazil

<sup>2</sup>Technomar Engineering, Av. Pedroso de Moraes, 631, São Paulo - SP, 05419-905, Brazil

<sup>3</sup>OSPL – Ocean Space Planning Laboratory, Department of Systems Innovation, School of Engineering, The University of Tokyo, 7-3-1 Hongo, Bunkyo-ku, Tokyo, 113-8656, Japan

## ABSTRACT

*The complex movements caused by ocean currents affecting floating offshore platforms, specifically Vortex-Induced Motion (VIM), are the focus of this study. It examines VIM patterns observed in towing tank experiments involving a scaled model of a Floating Offshore Wind Turbine (FOWT) with a 4-circular-column platform and pontoons. A simplified mathematical model (ROM) was applied to analyze VIM, considering horizontal plane motions such as in-line, transverse, and yaw. The ROM model represented current forces using “wake variables”, adapting existing models initially developed for VIM of single-column platforms. It comprised eleven generalized coordinates, covering three for rigid body motion on the horizontal plane and a pair of wake variables for each column, resulting in an eleven-nonlinear second-order system of Ordinary Differential Equations (ODEs). The wake variable pairs followed van der Pol equations, incorporating hydrodynamic coefficients and parameters derived from prior experiments with low-draft cylinders. To simplify the numerical model, the hydrodynamic interactions among columns were not considered. Its accuracy was evaluated through a case study involving a small-scale experimental campaign. Simulations were performed at two different current incidence angles (0 and 45 degrees) across various reduced velocities. The simulations replicated the observed oscillations in the experimental trials, demonstrating fair agreement in transverse and yaw oscillations, including lock-in phenomena.*

Keywords: VIM, FOWT, Reduced-order Model, Wake Oscillator modeling, experimental comparison.

## INTRODUCTION

With its favorable combination of power density, stability, and expansive oceanic areas, offshore wind has emerged as a promising renewable energy source. Tension Leg Platforms (TLPs), mono-columns, and semisubmersible (SS) platforms, originally designed for offshore oil and gas, are now utilized in offshore wind to support turbines in mid and deep waters [Error! Reference source not found.]. These floating structures endure significant loads from waves, wind, and currents, including oscillatory motions induced by ocean currents, known as Flow-Induced Motions (FIM) [2, 3].

Vortex-Induced Motions (VIM) is a particular case of the FIM, and it is a non-linear resonant phenomenon falling under the Vortex-Induced Vibration (VIV) category, where vortex structures synchronize with the natural frequencies of the floating platform. VIM is an issue for multi-column platforms, such as FOWT. This phenomenon can increase fatigue failure in the mooring and cable systems and may stop the turbine's operation. Unlike the high-frequency structural damage due to wave-induced motions (WIM), VIM causes low-frequency structural damage.

Most of the articles addressing the VIM phenomenon studied its importance by model tests at towing tanks. For example, among recent articles focusing on the experimental investigation of VIM of FOWT, the work by Gonçalves *et al.* [4] can be cited. The VIM of the benchmarking FOWT semi-submersible type (OC4 phase II) was investigated in that work. They showed amplitudes in the transverse direction of around 70% of the diameter of the platform column, which is similar to those observed for

deep-draft (DD) SS with circular columns. The results showed that as VIM occurred, its effect has to be considered in the mooring system and electric cable design due to large displacements in the horizontal plane in the operational phases and also relevant motions during the tow-out operations in the installation phases.

Moreover, the VIM started to play an important role when the FOWT designs included long horizontal pontoons due to significative motions in the vertical plane (heave, roll, and pitch) due to the VIM phenomenon, see Naito *et al.* [5]. Significant heave amplitudes, around 80% of the pontoon diameter, coupled with a maximum of 6 degrees of pitch and roll motions, were observed. The acceleration at the nacelle position due to the VIM may be able to stop the turbine operation and consequently diminish the efficiency of energy production; therefore, VIM also needs to be investigated in the design stages of FOWT.

Another way to evaluate the VIM is through Computational Fluid Dynamics (CFD) models, solving Navier-Stokes and Poisson equations. However, the extended computational time hinders its practicality in design, requiring thorough verification and validation [2, 3].

An alternative approach involves phenomenological models, like van der Pol equations, suited for vortex wake dynamics modeling. Aranha [4] demonstrated that the Ginsburg-Landau oscillators naturally emerge from the Navier-Stokes equations, a specific instance of the van der Pol equation.

The coupling of flow and structural dynamics for VIV is effectively represented by equations simulating classical VIV dynamics. Early models such as Iwan and Blevins [5] laid the foundation, with later modifications considering inertial terms and acceleration-based coupling schemes [8], [9], [10]. Recent discussions have revisited the added mass concept role in VIV, exemplified by the reinterpretation proposed by Bernitsas *et al.* [11]. Ogink and Metrikine [10] revisited the 1-DoF VIV model of Facchinetto *et al.* [8], relaxing assumptions and adjusting coupling parameters based on experimental observations. Franzini and Bunzel [11] extended this approach to 2-DoFs, including a second van der Pol oscillator as in [14].

CFD has been used to calibrate wake oscillator models, exploring the influence of mass ratio on response amplitudes [14]. These models have been successfully used for Monocolumn Production, Storage, and Offloading (MPSO) floating platforms [15], [16]. The low aspect ratio of the platform significantly influences vortex shedding frequency and the Strouhal number [17]. Advancements in modeling VIM for MPSO include a two-wake oscillators model, building on Franzini and Bunzel's [13] framework. A 5-DoF Reduced Order Model (ROM) addressed platform dynamics and VIM phenomena, achieving good agreement with experimental results [18]. Notably, mooring line dynamics are modeled analytically, revealing yaw motions induced by the VIM forces [19].

A ROM was developed by de Oliveira *et al.* [20] for a multicolumn FOWT platform considering 3-DoF associated with the rigid body motion of the platform on the horizontal plane. Also, a pair of wake oscillators is coupled to each platform column,

resulting in an 11-DoF model. To verify the ROM, a simulation campaign was performed to reproduce the experiments reported by Gonçalves *et al.* [4] of a reduced-scale model platform. The ROM reproduced amplitudes in the transverse direction and lock-in regions very well, also revealing a resonant yaw motion for high reduced velocities, referred to in the experiments by an increased trend in the yaw amplitudes [4]. Motivated by the results of de Oliveira *et al.* [20], a model to assess the susceptibility of multicolumn FOWT to VIM was presented by Pesce *et al.* [21]. That model was tested by comparing it with ROM results under a simulation campaign considering a full-scale platform with nonlinear mooring effects and catenary configuration [21].

The present paper incorporates pontoon hydrodynamic effects into the ROM developed in [20]. The subsequent sections of this paper are structured as follows: initially, the ROM is described, and the incorporation of pontoon drag effects into the model is detailed. Following this, the case studies are outlined, and the obtained results are discussed. Finally, conclusions are drawn, and avenues for future research are proposed.

## THE REDUCED-ORDER MATHEMATICAL MODEL

The work by de Oliveira *et al.* [20] provides detailed deductions for a comprehensive understanding of the Reduced-Order Model (ROM). The ROM specifically addresses the horizontal plane motion of the platform, treating it as a rigid body with 3-DoF (see Figure 1). Derived from Lagrange's equations, the ROM incorporates hydrodynamic interaction through a phenomenological model based on wake oscillators, with two oscillators assigned to each column. This expands the generalized coordinate vector to  $3 + 2N_c$  degrees of freedom, which  $N_c$  represents the number of columns.

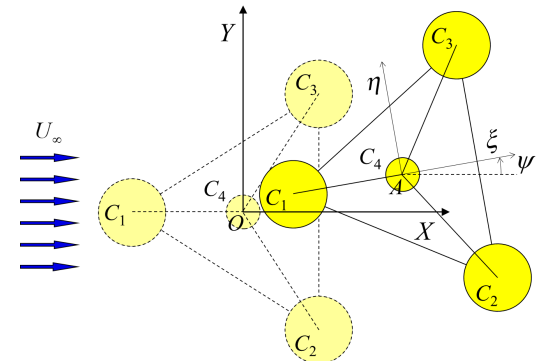


Figure 1. Coordinates and general definitions. At the origin, the platform is shown at 0 degrees current heading [20].

The 11-DoF reduced-order model may be written in the following form:

$$\tilde{\mathbf{M}}\ddot{\tilde{\mathbf{q}}} = \tilde{\mathbf{Q}}_c + \tilde{\mathbf{Q}}_{nc}, \quad (1)$$

where, on the l.h.s.,  $\tilde{\mathbf{M}}$  and  $\tilde{\mathbf{q}}$  are, respectively, the  $(11 \times 11)$  and  $(11 \times 1)$  augmented inertia matrix and generalized coordinate

vector; and on the r.h.s.,  $\tilde{\mathbf{Q}}_c$  and  $\tilde{\mathbf{Q}}_{nc}$  are, respectively, the  $(11 \times 1)$  generalized force vectors, the first one dependent on the generalized configuration of the system and the second one is a non-conservative term. Eq. (2) provides their respective forms explicitly.

$$\begin{aligned}\tilde{\mathbf{M}} &= \begin{bmatrix} \mathbf{M} & \mathbf{0} \\ \mathbf{A}_w & \mathbf{1} \end{bmatrix}; \quad \tilde{\mathbf{q}} = \begin{bmatrix} \mathbf{q} \\ \mathbf{w} \end{bmatrix}, \\ \tilde{\mathbf{Q}}_c &= \begin{bmatrix} \mathbf{Q}^m - \mathbf{Q}^I \\ \mathbf{Q}_w^r \end{bmatrix}; \quad \tilde{\mathbf{Q}}_{nc} = \begin{bmatrix} \mathbf{Q}^v + \mathbf{Q}_p^v \\ \mathbf{Q}_w^v \end{bmatrix},\end{aligned}\quad (2)$$

Where  $\mathbf{q}$  is the  $(3 \times 1)$  vector of generalized coordinates of the platform ( $X, Y, \psi$ );  $\mathbf{w}$  is the  $(8 \times 1)$  wake oscillators variables vector;  $\mathbf{M}$  is the  $(3 \times 3)$  inertia matrix of the platform, including rigid body and added mass parcels;  $\mathbf{A}_w$  is the  $(8 \times 8)$  matrix of inertial terms coupling the oscillators variables with the columns centers kinematics;  $\mathbf{Q}^m$ ,  $\mathbf{Q}^I$ ,  $\mathbf{Q}^v$ ,  $\mathbf{Q}_p^v$  are, respectively, the  $(3 \times 1)$  vectors associated to the generalized mooring forces, centrifugal/Coriolis effects, vortical viscous forces and pontoons drag;  $\mathbf{Q}_w^r$  and  $\mathbf{Q}_w^v$  are the corresponding  $(8 \times 1)$  vectors of restoring and damping effects related to the wake oscillators dynamics.

The wake oscillators model for each  $k$ -th column,  $k = 1, \dots, N_c$ , is written in the respective local in-line and transverse directions  $(\xi, \eta)$ , as presented below:

$$\begin{aligned}\ddot{w}_{\xi,k} + \varepsilon_\xi \omega_{s,k} (w_{\xi,k}^2 - 1) \dot{w}_{\xi,k} + 4\omega_{s,k}^2 w_{\xi,k} &= \frac{A_\xi}{D_k} a_{\xi,k}, \\ \ddot{w}_{\eta,k} + \varepsilon_\eta \omega_{s,k} (w_{\eta,k}^2 - 1) \dot{w}_{\eta,k} + \omega_{s,k}^2 w_{\eta,k} &= \frac{A_\eta}{D_k} a_{\eta,k},\end{aligned}\quad (3)$$

where  $w_{\xi,k}$  and  $w_{\eta,k}$  ( $k = 1, \dots, N$ ) are hidden generalized coordinates that phenomenologically emulate the wake dynamics and its interaction with the structure;  $\varepsilon_\xi$  and  $\varepsilon_\eta$  are damping parameters;  $A_\xi$  and  $A_\eta$  are the inertial coupling parameters;  $D_k$  is the column diameter;  $a_{\xi,k}$  and  $a_{\eta,k}$  are the body-fixed components of the columns accelerations and  $\omega_{s,k} = 2\pi S_{t,k} (U_k / D_k)$  is the shedding frequency, being  $S_{t,k}$  a characteristic value of the Strouhal number, specific for the case of low aspect ratio cylinders, and  $U_k$  is the relative velocity of the column center with respect to the flow. Notice that the in-line wake oscillator vibrates with twice the frequency corresponding to the crosswise one. This is a common *ad-hoc* assumption that comes from well-known experimental VIV observations, according to which the fundamental harmonic of drag forces pulsates twice as fast as that of the lift forces. The terms on the r.h.s. of Eq. (3) represent the coupling between the wake oscillators and the body equations of motion. The inertial coupling recommended in [5] has been followed by several authors, such as [12, 13]. The coefficients  $(\varepsilon_\xi, \varepsilon_\eta)$  and  $(A_\xi, A_\eta)$  have been calibrated from experiments obtained in [15, 16], and from CFD simulations in [14].

## Pontoons drag forces

The contributions of the pontoons to the added mass tensor have already been considered and included in the inertial terms in Eq. (2), but not the hydrodynamic damping, which is done in the present section. The drag forces related to the pontoons can be modeled in terms of their components in the body-fixed coordinate system using the Strip Theory. So, let  $U_\infty$  be the free stream velocity, which is supposed to be aligned with the axis  $OX$ . Also, let  $U_{s,l}$  be the instantaneous relative velocity of the current stream with respect to the centroid of the  $s$ -th strip on the  $l$ -th pontoon, being  $U_{\xi,s,l}$  and  $U_{\eta,s,l}$ , their projections on the axes. Define  $F_{v_{\xi,s,l}}$  and  $F_{v_{\eta,s,l}}$  as the components of the drag force in the directions  $\xi_{s,l}$  and  $\eta_{s,l}$ , respectively.

Considering a platform with  $N_p$  pontoons, each one of them divided into  $N_s$  strips, such that  $l = 1, \dots, N_p$  and  $s = 1, \dots, N_s$ , we then follow [9] and [20], to obtain:

$$\begin{aligned}U_{\xi,s,l} &= U_{\infty,\xi,s,l} - v_{\xi,s,l}; \quad U_{\eta,s,l} = U_{\infty,\eta,s,l} - v_{\eta,s,l}, \\ U_{s,l} &= \sqrt{U_{\xi,s,l}^2 + U_{\eta,s,l}^2}.\end{aligned}\quad (4)$$

The velocity terms are expressed in the local frame of the respective strip,  $(C_{s,l}, \xi_{s,l}, \eta_{s,l})$ , such that  $U_{\infty,\xi,s,l}$  and  $U_{\infty,\eta,s,l}$  are the components of the stream velocity, whereas  $v_{\xi,s,l}$  and  $v_{\eta,s,l}$  are the components of the velocity vector of the  $s$ -th strip center along the  $l$ -th pontoon, i.e.:

$$\mathbf{v}_{s,l} = \mathbf{v}_A + \boldsymbol{\omega}_p \times \mathbf{r}_{s,l}, \quad (5)$$

where  $\mathbf{v}_A$  is the velocity vector of the centroid of the platform,  $A$ , on the horizontal plane,  $\boldsymbol{\omega}_p$  is the angular velocity vector of the platform, and  $\mathbf{r}_{s,l}$  is the relative position vector between  $A$  and the center of the  $s$ -th strip on the  $l$ -th pontoon.

The components  $F_{v_{\xi,s,l}}$  and  $F_{v_{\eta,s,l}}$  are written as follows [20]:

$$F_{v_{\xi,s,l}} = \frac{1}{2} \rho \delta_{s,l} H_l C_{D,l} U_{\xi,s,l} U_{s,l}; \quad F_{v_{\eta,s,l}} = \frac{1}{2} \rho \delta_{s,l} H_l C_{D,l} U_{\eta,s,l} U_{s,l}, \quad (6)$$

where  $\rho$  is the density of the water,  $\delta_{s,l}$  is the strip length,  $H_l$  is the pontoon height and  $C_{D,l}$  is the sectional drag coefficient.

The corresponding generalized drag force vector related to the pontoons turns out to be:

$$\mathbf{Q}_p^v = \left[ Q_{p,j}^v \right]; \quad Q_{p,j}^v = \sum_{l=1}^{N_p} \sum_{s=1}^{N_s} \mathbf{F}_{v,s,l} \cdot \frac{\partial \mathbf{v}_{s,l}}{\partial q_j}; \quad j = 1, 2, 3. \quad (7)$$

## A CASE STUDY

To verify the applicability of the model, a case study was carried out considering the reduced-scale model (1:100) of the CC platform (Figure 2) with a simplified mooring system composed of 4 springs lines connected to the towing carriage (Figure 3), used by Gonçalves *et al.* [23]. The experimental model was composed of four main circular columns in an equilateral arrangement. The results presented herein replicate the experiments on a reduced scale, where two current incidence angles were considered (0 and 45 degrees), as illustrated in Figure 3(b) and (c).

The numerical simulations were carried out at least for 30 reduced velocities, spanning the range  $4 < V_R < 30$ , which corresponds to the Reynolds number range  $7,000 < Re < 80,000$ , for each incidence angle. The simulations were carried out in a MATLAB® environment, numerically integrating the coupled equations in the state space form. A fixed time step of 0.1 seconds was used, applying the 4<sup>th</sup>-order Runge-Kutta algorithm.

The platform and pontoons parameters are shown in Tables 1 and 2, respectively, while the wake oscillator parameters are given in Table 3. Table 4 shows the inertia and stiffness matrices calculated at the trivial equilibrium position for the current incidences considered in the small-scale experiment, while Table 5 shows the three natural periods evaluated at the same trivial equilibrium condition, comparing those experimentally measured with those calculated with the ROM. Notice that the oscillation modes are pure at the trivial equilibrium, uncoupling the  $(X, Y, \psi)$  degrees of freedom. As the platform model drifts off from that trivial equilibrium position, mooring stiffnesses change, and motions become coupled to each other, hence producing yaw, even if the current is originally aligned with an axis of symmetry.

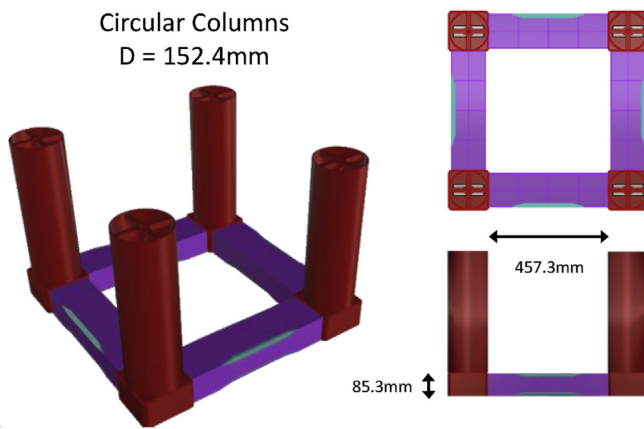


Figure 2. Sketch of the CC platform model scaled in 1:100 with the main dimensions indicated [23].

The added mass tensor components in Table 1 were calculated by performing an analysis with Ansys® Aqwa at the trivial equilibrium position for the asymptotic limit of null frequency.

The stiffness matrix in Table 4 was used to model the mooring system effect in the simulations. This simplification was performed due to the weak nonlinearity presented in the mooring system adopted in [23].

Table 1. CC scaled model parameters [23].

Parameters	Values
Draught, $H$ [m]	0.250
Arc radius, $R$ [m]	0.539
Columns centers' radius, $r$ [m]	0.463
Diameters, $\{D_1, D_2, D_3, D_4\}$ [m]	{0.1524, 0.1524, 0.1524, 0.1524}
Platform's mass matrix, $\mathbf{M}_p$ [kg, kg, kgm <sup>2</sup> ]	diag{45.10, 45.10, 6.85}
Local added mass tensor, $\hat{\mathbf{M}}_a$ [kg, kg, kgm <sup>2</sup> ]	diag{32.22, 32.22, 4.16}
Density of water, $\rho$ [kg/m <sup>3</sup> ]	997

Table 2. Pontoon parameters [23].

Parameters	Values
Sectional drag coefficients, $C_D$	0.61
Pontoon height, $H_l$ [m]	0.085
Strips length, $\delta_s$ [m]	0.076
Strips per pontoons, $N_s$	10

Table 3. Wake-oscillator parameters [15, 24].

Parameters	Values
$\{A_\xi, A_\eta\}$	{12, 6}
$\{\varepsilon_\xi, \varepsilon_\eta\}$	{0.30, 0.15}
$\{C_{D0}, C_{L0}, C_{D0}^f, K\}$	{0.70, 0.30, 0.10, 0.05}
Strouhal numbers for each column, $\{S_{t_1}, S_{t_2}, S_{t_3}, S_{t_4}\}$	{0.144, 0.144, 0.144, 0.144}

Table 4. Mass and stiffness matrices at the trivial equilibrium position [23].

Incidence	$0^\circ$		$45^\circ$	
	Mass matrix, $\mathbf{M}$ [kg, kg, kgm <sup>2</sup> ]	diagonal {77.33, 77.33, 11}	Mooring stiffness matrix, $\mathbf{K}$ [N/m, N/m, Nm/rad]	diagonal {21.2, 21.2, 15.46}
$0^\circ$				
$45^\circ$				

Table 5. Natural periods at the origin [23].

Incidence	Experiment		ROM	
	$0^\circ$	$45^\circ$	$0^\circ$	$45^\circ$
DOF	$T_n$ [s]	$T_n$ [s]	$T_n$ [s]	$T_n$ [s]
$X$	12.0	12.0	12.1	12.1
$Y$	12.0	12.0	12.1	12.1
$\psi$	5.3	5.3	5.3	5.3

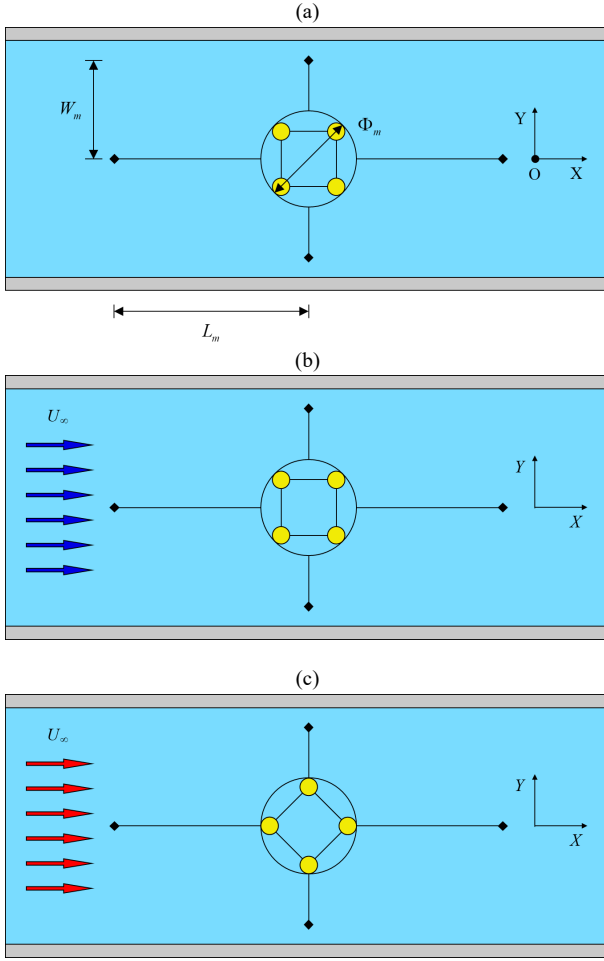


Figure 3. Experiment sketch with the simplified mooring. (a): Tank sketch and mooring system geometry. (b) and (c): Incoming flow incidence at 0 and 45 degrees. Adapted from [20].

An interesting way to observe the behavior of the platform centroid concerning the main flow in the  $Y$ -direction (transverse, or cross-wise), and  $X$ -direction (in-line) is by showing its trajectories on the horizontal plane [4]. For that, Figures 4 and 5 illustrate the trajectory of the centroid of the platform on the horizontal plane considering or not drag forces on the pontoons. Yaw motion was represented by the colored bar. The results were obtained with the ROM for the current incidences considered and for a sample of the reduced velocities of the experiment.

The reduced velocity sample was chosen considering the synchronization range of the platform oscillations in the transverse direction and the yaw angle. All simulations started from rest at the trivial equilibrium position.

Figures 6 and 7 compare the nondimensional amplitudes predicted by the proposed ROM with and without drag on the pontoons and the experimental results presented in [23]. Figure

6(a) shows that the proposed ROM produced a realistic representation of the transverse oscillation amplitude ( $A_Y / D$ ) for the incidence of 0 degrees, with maximum oscillation amplitude (0.42 at  $V_R \sim 8$ ) close to the one observed experimentally (0.46 at  $V_R \sim 9$ ) when the pontoons drag was considered. Otherwise, the ROM overpredicted the transverse amplitude (0.64 at  $V_R \sim 9$ ). The synchronization range obtained with the ROM ( $5 < V_R < 14$ ) also approximated well the one observed in the experiments ( $5 < V_R < 12$ ), being very similar for the two cases considered, with and without pontoons drag.

For the 45-degree incidence case, the transverse oscillation was well represented, as seen in Figure 7(a). In this case, the maximum oscillation amplitude determined with the ROM considering pontoon drag (0.42 at  $V_R \sim 8$ ) was slightly different from that observed in the experiment (0.33 at  $V_R \sim 7$ ). In contrast, the amplitude calculated with the ROM disconsidering pontoon drag (0.64 at  $V_R \sim 9$ ) overpredicted the experiment. The synchronization range predicted by the models ( $5 < V_R < 13$ ) was wider than the one observed experimentally ( $5 < V_R < 10$ ).

Regarding the amplitude of the in-line oscillation ( $A_X / D$ ), both models approximated the magnitude of the experimental results at the beginning of the crosswise oscillation synchronization range for all the incidence angles analyzed. It should be noticed that the wake interference may be conceived as relatively weak at small reduced velocities. Notice also that the graphs of dominant frequencies revealed, quite clearly, switches between oscillation modes, with jumps occurring at reduced velocities close to 5 and 15.

In the yaw oscillation amplitude ( $A_\psi$ ) at 0-degree incidence shown in Figure 6(c), the ROM considering pontoons drag predicted a maximum value of 4.4 degrees at  $V_R \sim 15$ , overestimating the typical values found in the experiment, around 3 degrees. The overprediction was even larger for the ROM without pontoon drag, with a maximum value of 7 degrees at  $V_R \sim 16$ . In the case of 45 degrees depicted in Figure 7(c), the ROM considering pontoons drag foresaw a maximum value of 1.8 degrees at  $V_R \sim 17$ , underestimating the typical value of the experiment, around 3.4 degrees. In the case of the ROM disconsidering pontoon drag, the maximum predicted value was around 2.9 degrees at  $V_R \sim 16$ , closer to the one found in the experiment.

In fact, beyond the main synchronization – the lock-in range for the oscillations in the transverse direction – an interesting behavior was revealed by the simulations and confirmed by the experiments: a resonant response of the yaw angle. Indeed, looking at Table 5, the yaw natural period at the trivial equilibrium position was grossly half the other two. A VIV-like resonance regime would appear if the graphs of yaw amplitude response and respective dominant frequencies were replotted by redefining the reduced velocity parameter based on the yaw natural frequency.

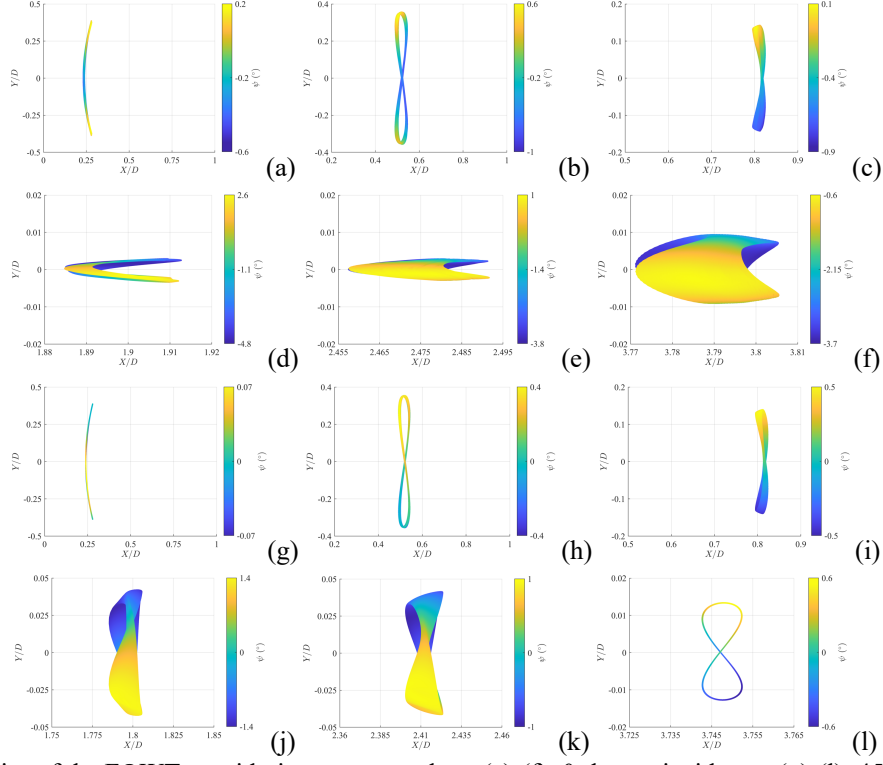


Figure 4. Trajectories of the FOWT considering pontoons drag. (a)-(f): 0-degree incidence; (g)-(l): 45-degrees incidence; (a) & (f):  $V_R = 6.29$ ; (b) & (h):  $V_R = 9.45$ ; (c) & (i):  $V_R = 12.59$ ; (d) & (j):  $V_R = 18.89$ ; (e) & (k):  $V_R = 22.04$ ; (f) & (l):  $V_R = 27.55$ .

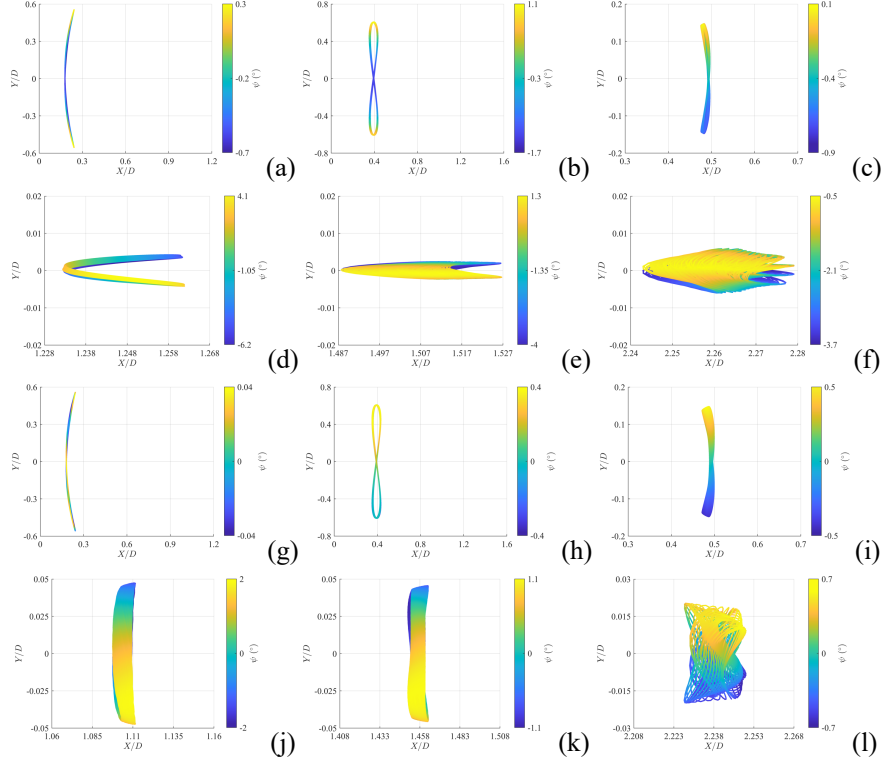


Figure 5. Trajectories of the FOWT dis considering pontoons drag. (a)-(f): 0-degree incidence; (g)-(l): 45-degrees incidence; (a) & (f):  $V_R = 6.29$ ; (b) & (h):  $V_R = 9.45$ ; (c) & (i):  $V_R = 12.59$ ; (d) & (j):  $V_R = 18.89$ ; (e) & (k):  $V_R = 22.04$ ; (f) & (l):  $V_R = 27.55$ .

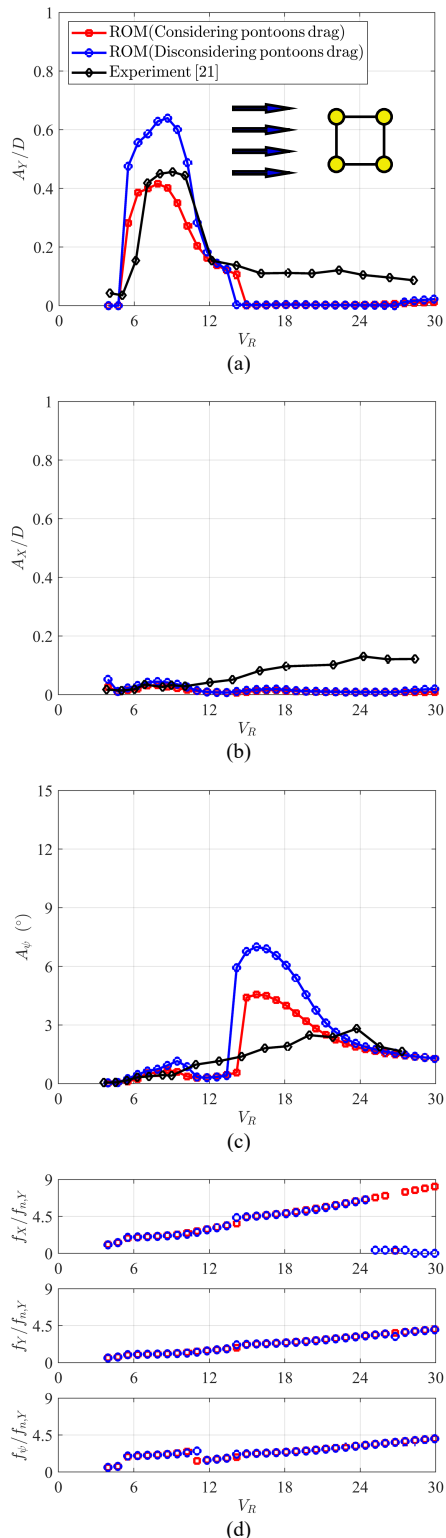


Figure 6. Comparison with experimental results, [23]. Flow at 0 degree. (a): Transverse amplitude; (b): In-line amplitude; (c): Yaw amplitude; (d): Dominant nondimensional frequencies.

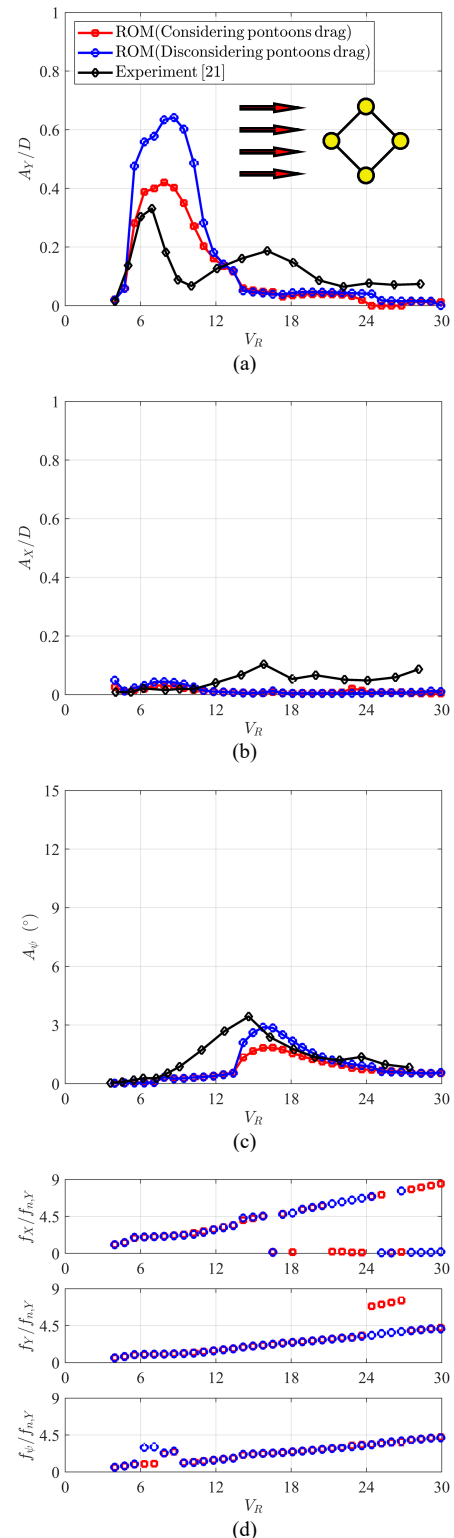


Figure 7. Comparison with experimental results [23]. Flow at 45 degrees. (a): Transverse amplitude; (b): In-line amplitude; (c): Yaw amplitude; (d): Dominant nondimensional frequencies.

## CONCLUSIONS

A mathematical ROM [20] was worked out and applied to address the VIM of a moored multicolumn FOWT platform with pontoons, focusing on slow horizontal motions at low frequencies. The ROM considered the approximated asymptotic values of the added mass tensor at zero frequency. Viscous fluid forces arising from vortex shedding were phenomenologically modeled using a pair of van der Pol-type wake oscillators, which captured the dynamics of the vortex wake shed from each cylindrical column. These oscillators responded to the local relative velocity of the incoming flow about the centroid of each column. The model simplified the analysis by neglecting wake interactions between columns. Parameters for the wake oscillators were derived from the technical literature, while Strouhal numbers were based on experimental data obtained for cylinders with a low-aspect ratio.

The ROM validation performed through reduced-scale experiments showed reasonably good agreement, particularly regarding transverse and yaw oscillations across various current incidence angles. Despite some differences when comparing model predictions with experimental findings and the simplifications inherent in the mathematical formulation, the results indicated the potential of the ROM. This is especially true when adding the pontoon drag forces in the formulation, which produced better predictions.

Further work might incorporate the effects of wake interactions between columns and conduct parametric sensitivity analyses concerning hydrodynamic parameters. Such improvements aim to refine ROM accuracy and broaden its applicability in predicting the response of multicolumn FOWT platforms. Based on first principles, ROMs are especially useful in the design phases, allowing expeditious analyses to be carried out, which can be easily included in optimization procedures.

## ACKNOWLEDGEMENTS

The Petrobras Deep Water Floating Offshore Wind Turbine project is acknowledged for partially supporting the present work. The second author acknowledges a research grant from CNPq, process 307995/2022-4, as well as the FAPESP thematic project ‘Nonlinear dynamics applied to engineering problems’, process 2022/00770-0.

## REFERENCES

1. H. Díaz, J. Serna, J. Nieto, and C. G. Soares, “Market Needs, Opportunities and Barriers for Floating Wind Industry,” *Journal of Marine Science and Engineering*, vol. 10, 934, 2022, doi:10.3390/jmse10070934.
2. A. L. C. Fujarra, G. F. Rosetti, J. de Wilde, and R. T. Gonçalves, “State-of-Art on Vortex-Induced Motion: A Comprehensive Survey After More Than One Decade of Experimental Investigation,” in *Volume 4: Offshore Geotechnics; Ronald W. Yeung Honoring Symposium on Offshore and Ship Hydrodynamics*, American Society of Mechanical Engineers, Jul. 2012, pp. 561–582. doi: 10.1115/OMAE2012-83561.
3. D. Yin, E. Passano, F. Jiang, H. Lie, J. Wu, N. Ye, S. Saevik and B. J. Leira, “State-of-the-art review of vortex-induced motions of floating offshore wind turbine structures,” *Journal of Marine Science and Engineering*, vol. 10, pp. 1021, 2020, doi: 10.3390/jmse10081021.
4. R. T. Gonçalves, M. E. F. Chame, L. S. P. Silva, A. Koop, S. Hirabayashi, and H. Suzuki, “Experimental Flow-Induced Motions of a FOWT Semi-Submersible Type (OC4 Phase II Floater),” in *Journal of Offshore Mechanics and Arctic Engineering*, American Society of Mechanical Engineers, vol. 143, pp. 012004, Feb. 2021. doi: 10.1115/1.4048149.
5. Y. Naito, S. Hirabayashi, H. Suzuki and R. T. Gonçalves, “Experimental study on flow-induced pitch, roll and heave motions of a semi-submersible floater with long pontoons,” In *Proceedings of the ASME 2023 42nd International Conference on Ocean, Offshore and Arctic Engineering*, OMAE2023-104664, Melbourne, Australia, 2023.
6. J. A. P. Aranha, “Weak three dimensionality of a flow around a slender cylinder: The ginzburg-landau equation,” *Journal of the Brazilian Society of Mechanical Sciences and Engineering*, vol. 26, no. 4, pp. 355–367, 2004, doi: 10.1590/S1678-58782004000400002.
7. W. D. Iwan and R. D. Blevins, “A Model for Vortex Induced Oscillation of Structures,” *J Appl Mech*, vol. 41, no. 3, pp. 581–586, Sep. 1974, doi: 10.1115/1.3423352.
8. M. L. Facchinetto, E. de Langre, and F. Biolley, “Coupling of structure and wake oscillators in vortex-induced vibrations,” *J Fluids Struct*, vol. 19, no. 2, pp. 123–140, Feb. 2004, doi: 10.1016/j.jfluidstructs.2003.12.004.
9. A. L. C. Fujarra and C. P. Pesce, “Added Mass Variation and Van der Pol Models Applied to Vortex-Induced Vibrations,” in *5th International Symposium on Fluid Structure Interaction, Aeroelasticity, and Flow Induced Vibration and Noise*, ASMEDC, Jan. 2002, pp. 207–211. doi: 10.1115/IMECE2002-32162.
10. L. D. Cunha, C. P. Pesce, J. Wanderley, and A. L. C. Fujarra, “The Robustness of the Added Mass in VIV Models,” in *Vol-*

- ume 4: Terry Jones Pipeline Technology; Ocean Space Utilization; CFD and VIV Symposium*, ASMEDC, Jan. 2006, pp. 731–738. doi: 10.1115/OMAE2006-92323.
11. M. M. Bernitsas, J. Ofuegbé, J.-U. Chen, and H. Sun, “Eigen-Solution for Flow Induced Oscillations (VIV and Galloping) Revealed at the Fluid-Structure Interface,” in *Volume 2: CFD and FSI*, American Society of Mechanical Engineers, Jun. 2019. doi: 10.1115/OMAE2019-96823.
  12. R. H. M. Ogink and A. V. Metrikine, “A wake oscillator with frequency dependent coupling for the modeling of vortex-induced vibration,” *J Sound Vib*, vol. 329, no. 26, pp. 5452–5473, Dec. 2010, doi: 10.1016/j.jsv.2010.07.008.
  13. G. R. Franzini and L. O. Bunzel, “A numerical investigation on piezoelectric energy harvesting from Vortex-Induced Vibrations with one and two degrees of freedom,” *J Fluids Struct*, vol. 77, pp. 196–212, Feb. 2018, doi: 10.1016/j.jfluidstructs.2017.12.007.
  14. A. Postnikov, E. Pavlovskaia, and M. Wiercigroch, “2DOF CFD calibrated wake oscillator model to investigate vortex-induced vibrations,” *Int J Mech Sci*, vol. 127, no. May 2016, pp. 176–190, Jul. 2017, doi: 10.1016/j.ijmecsci.2016.05.019.
  15. G. F. Rosetti, R. T. Gonçalves, A. L. C. Fujarra, K. Nishimoto, and M. D. Ferreira, “A Phenomenological Model for Vortex-Induced Motions of the Monocolumn Platform and Comparison with Experiments,” in *Volume 1: Offshore Technology*, ASMEDC, Jan. 2009, pp. 437–444. doi: 10.1115/OMAE2009-79431.
  16. G. F. Rosetti, R. T. Gonçalves, A. L. C. Fujarra, and K. Nishimoto, “Parametric analysis of a phenomenological model for vortex-induced motions of monocolumn platforms,” *Journal of the Brazilian Society of Mechanical Sciences and Engineering*, vol. 33, no. 2, pp. 139–146, Jun. 2011, doi: 10.1590/S1678-58782011000200004.
  17. R. T. Gonçalves, F. T. Matsumoto, E. B. Malta, G. F. Rosetti, A. L. C. Fujarra, and K. Nishimoto, “Evolution of the MPSO (monocolumn production, storage and offloading system),” *Marine Systems & Ocean Technology*, vol. 5, no. 1, pp. 45–53, Dec. 2009, doi: 10.1007/BF03449242.
  18. B. A. Pesce, É. L. de Oliveira, and C. P. Pesce, “Vortex Induced Motions of a Moored Monocolumn Platform,” in *DINAME2019*, ABCM, 2019. doi: 10.26678/ABCM.DINAME2019.DIN2019-0213.
  19. C. P. Pesce, G. A. Amaral, and G. R. Franzini, “Mooring System Stiffness: A General Analytical Formulation with an Application to Floating Offshore Wind Turbines,” in *ASME 2018 1st International Offshore Wind Technical Conference*, American Society of Mechanical Engineers, Nov. 2018. doi: 10.1115/IOWTC2018-1040.
  20. É. L. de Oliveira, C. P. Pesce, B. Mendes, R. M. M. Orsino, and G. R. Franzini, “A Reduced-Order Mathematical Model for the Current-Induced Motion of a Floating Offshore Wind Turbine,” in *ASME 2021 3rd International Offshore Wind Technical Conference*, American Society of Mechanical Engineers, Feb. 2021, pp. 1–11. doi: 10.1115/IOWTC2021-3503.
  21. C. P. Pesce, G. A. Amaral, B. Mendes, É. L. Oliveira, and G. R. Franzini, “A Model to Assess the Susceptibility of a Multicolumn FOWT Platform to Vortex-Induced Motions in Early Design Stages,” in *Volume 9: Ocean Renewable Energy*, American Society of Mechanical Engineers, Jun. 2021, pp. 1–10. doi: 10.1115/OMAE2021-65761.
  22. M. J. Slingsby, “Dynamic interaction of subsea pipeline spans due to vortex-Induced Vibrations,” Master Thesis, Delft University of Technology, 2015. [Online]. Available: <http://resolver.tudelft.nl/uuid:329c686e-ef05-4849-a4a8-64ae327eb215>
  23. R. T. Gonçalves, A. L. C. Fujarra, G. F. Rosetti, A. M. Kogishi, and A. Koop, “Experimental study of the column shape and the roughness effects on the vortex-induced motions of deep-draft semi-submersible platforms,” *Ocean Engineering*, vol. 149, pp. 127–141, Feb. 2018, doi: 10.1016/j.oceaneng.2017.12.013.
  24. R. T. Gonçalves, G. R. Franzini, G. F. Rosetti, J. R. Meneghini, and A. L. C. Fujarra, “Flow around circular cylinders with very low aspect ratio,” *J Fluids Struct*, vol. 54, pp. 122–141, Apr. 2015, doi: 10.1016/j.jfluidstructs.2014.11.003.